



**HAL**  
open science

## Reduced-order LPV controller for coordination of power sources within multi-source energy systems

Waleed Nwesaty, Antoneta Iuliana Bratcu, Olivier Sename

### ► To cite this version:

Waleed Nwesaty, Antoneta Iuliana Bratcu, Olivier Sename. Reduced-order LPV controller for coordination of power sources within multi-source energy systems. ROCOND 2015 - 8th IFAC Symposium on Robust Control Design, International Federation of Automatic Control (IFAC), Jul 2015, Bratislava, Slovakia. pp.131-136, 10.1016/j.ifacol.2015.09.446 . hal-01150179

**HAL Id: hal-01150179**

**<https://hal.science/hal-01150179>**

Submitted on 2 Aug 2016

**HAL** is a multi-disciplinary open access archive for the deposit and dissemination of scientific research documents, whether they are published or not. The documents may come from teaching and research institutions in France or abroad, or from public or private research centers.

L'archive ouverte pluridisciplinaire **HAL**, est destinée au dépôt et à la diffusion de documents scientifiques de niveau recherche, publiés ou non, émanant des établissements d'enseignement et de recherche français ou étrangers, des laboratoires publics ou privés.

# Reduced-order LPV controller for coordination of power sources within multi-source energy systems

W. Nwesaty, A. I. Bratcu, O. Sename

Grenoble Institute of Technology, GIPSA-lab, Control Systems  
Department, 38402, Saint-Martin d'Herès, France. e-mail:  
(waleed.nwesaty, antoneta.bratcu, olivier.sename)  
@gipsa-lab.grenoble-inp.fr

---

Abstract: In this paper an order-reduction approach for multi-variable LPV/ $H_\infty$  controller is presented and applied to design a power source coordination strategy within a multi-source energy system. The energy system has three different kinds of power sources – fuel cell, battery and supercapacitor – which compose the power supply system of an electric vehicle. All sources are paralleled together with their associated DC-DC converters on a common DC-link coupled to vehicle's electrical motor and its converter. DC-link voltage must be regulated in spite of load power variations corresponding the driving cycle. A reduced LPV controller is obtained using the ISTIA algorithm. It shows to have a special form consistent with the physical properties of the studied system. The MIMO LPV reduced controller is proved to ensure quadratic stability of the closed-loop system. Besides, this controller could be implemented with smaller computational burden. The nonlinear multi-source system is simulated in MATLAB<sup>®</sup>/Simulink<sup>®</sup> using the Normalized European Driving Cycle (NEDC) as load profile. Simulation shows good performance of the reduced-order LPV/ $H_\infty$  controller to be used in power sharing strategy.

Keywords:  $H_\infty$  control, LPV systems, power source coordination, frequency separation, electric vehicle.

---

## 1. INTRODUCTION

Lots of studies are concerned today with the combination different electric power sources within the vehicles such as fuel cell, battery, photovoltaic sources and supercapacitors, *etc...*, maximizing the energy efficiency. Moreover fuel cell could be combined with battery and supercapacitor in order to achieve the same power and energy density similar to an ordinary internal combustion engine (Hannan et al. [2011]).

There are two terms to describe a power source with respect to its power supply ability according to Ragone's classification (Kuperman and Aharon [2011]): source with high power density, which is able to provide high power for a short period of time with high dynamic characteristics (supercapacitors are typical examples of such type of sources), and source with high energy density, which is able to provide power during long periods of time with slow dynamic characteristics (fuel cells and batteries belong to this class of sources).

Many configuration topologies can be proposed regarding number of components, energy management complexity, and performance reliability. There are three main topological architectures: series, parallel, and cascaded (Aharon and Kuperman [2011], Tie and Tan [2013]). In this paper, the parallel structure is chosen due to its flexibility to adapt system parameters such that DC-bus voltage value, sources' independence, and even the facility to replace or to add more power sources (photo-voltaic panels, grid electricity, *etc...*). In this structure, each power source is

associated to a DC-DC converter then all converters are connected in parallel to a DC-bus in order to satisfy the vehicle power demand.

In the literature, a significant number of power source coordination strategies can be found which aim to regulate DC-bus voltage, such that proportional-integral controllers (Wong et al. [2011]), fuzzy logic control (Fadel and Zhou [2011]), filtering strategy (Florescu et al. [2015]), and LQG optimal control (Florescu et al. [2014]). However, there is still lack of proof for closed-loop stability and robust performance.

This paper presents further results related to the strategy proposed by the authors in Nwesaty et al. [2014], where an LPV/ $H_\infty$  control is applied to power sources coordination in order to guarantees quadratic stability for closed-loop system. In this strategy, power sources are coordinated in a manner related to frequency specification of each one, which protects fuel cell and battery from high variation in power demand and in consequence prolong their lifetimes, and uses the supercapacitor to handle instantaneous to/from power to the DC-bus. However, the obtained LPV/ $H_\infty$  controller is quite complex since it is a convex combination between eight vertex controllers, and each of which is an eighteen-order LTI system.

This paper presents an order reduction solution for the MIMO/LPV controller. The Iterative SVD Tangential Krylov Algorithm (ISTIA) (Poussot-Vassal and Vuillemin [2012]) is here used in order to reduce the complexity of

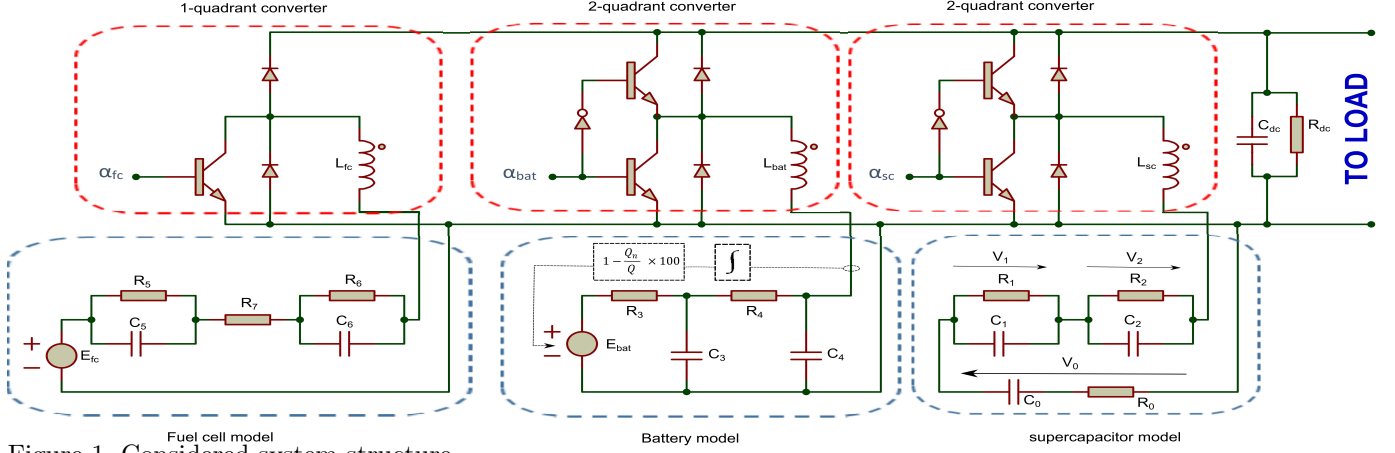


Figure 1. Considered system structure.

all vertex controllers. The global stability of the closed-loop LPV system is proved a posteriori finding a single Lyapunov function that satisfies  $A_i^T P + P A_i < 0$ , where  $P > 0$  and  $A_i$  are the closed-loop system at the polytope vertices. It is worth noting that the reduced-order controller is shown to be able to cope with the system's properties and satisfies its physical constraints. Finally the authors would like to stress that the presented method uses known tools and mathematically proved algorithms in order to propose a generic solution that can be applied for any similar system potentially with any number of power sources.

This paper is structured as follows. Section 2 discusses the system model, control objectives and presents the  $LPV/H_\infty$  control solution. The order reduction is detailed in Section 3. Section 4 is dedicated to frequency analysis of the reduced-order controller. The simulation results are outlined and discussed in Section 5. Lastly, in Section 6, conclusion and future work are presented.

## 2. SYSTEM MODEL, CONTROL OBJECTIVES, AND $LPV/H_\infty$ CONTROL DESIGN

### 2.1 Electrical system model

The full electrical scheme of the system is represented in Fig. 1. The DC-bus voltage is supposed to be regulated to a desired reference value (150 V). To this end, a capacitor  $C_{dc}$  is added to the output in order to investigate its dynamic. Supercapacitor's state of charge (SOC) is also required to be maintained within admissible limit. Fuel cell and battery are considered as current sources where their internal dynamics are not controlled. The DC-DC converters are regulated using a PI-controller for each one (Fig. 2), these internal control loops are tuned to be faster than  $LPV/H_\infty$  control one and considered to be transparent layer to the main control strategy (Aström and Hägglund [1995]) (Fig. 2). Using Kirchhoff's circuit laws, the system can be modelled by the following state-space representation (see Nwesaty et al. [2014] for more details):

$$\begin{cases} \dot{x} = A.x + B_1.\omega + B_2(\rho).u \\ y = C.x + D.u \end{cases} \quad (1)$$

where the state vector  $x = [V_{DC} \ V_1 \ V_2 \ V_0]^T$  consists of the DC-bus voltage and the sub-voltages represented in supercapacitor model, respectively.  $\omega = I_{Load}$

is load current which represents the disturbance input,  $u = [I_{fc} \ I_{bat} \ I_{sc}]^T$  is the control input vector composed of fuel cell, battery and supercapacitor currents respectively.  $\rho = [\rho_1 \ \rho_2 \ \rho_3]^T = [\alpha_{fc} \ \alpha_{bat} \ \alpha_{sc}]^T$  is the parameter vector represented by converters' averaged duty cycles (averaged pulse width modulation command signals). Matrices in (1) are:

$$A = \begin{bmatrix} -1 & 0 & 0 & 0 \\ \frac{C_{dc}R_{dc}}{C_{dc}R_{dc}} & -1 & 0 & 0 \\ 0 & \frac{-1}{C_1R_1} & 0 & 0 \\ 0 & 0 & \frac{-1}{C_2R_2} & 0 \\ 0 & 0 & 0 & 0 \end{bmatrix}$$

$$B_1 = \begin{bmatrix} -1 \\ \frac{C_{dc}}{C_{dc}} \\ 0 \\ 0 \\ 0 \end{bmatrix}, \quad B_2 = \begin{bmatrix} 1 - \rho_1 & \rho_2 & \rho_3 \\ C_{dc} & C_{dc} & C_{dc} \\ 0 & 0 & \frac{-1}{C_1} \\ 0 & 0 & \frac{-1}{C_2} \\ 0 & 0 & \frac{-1}{C_0} \end{bmatrix}$$

$$C = \begin{bmatrix} 1 & 0 & 0 & 0 \\ 0 & 1 & 1 & 1 \end{bmatrix}, \quad D = \begin{bmatrix} 0 & 0 & 0 \\ 0 & 0 & -R_0 \end{bmatrix}$$

where  $C_{dc}$  and  $R_{dc}$  are the DC-bus capacitor and resistance respectively.  $R_0, C_0, R_1, C_1, R_2$  and  $C_2$  are constant parameters of supercapacitor model (Fig. 1).

### 2.2 Control objectives

- (1) Regulate DC-bus voltage at  $150V \pm 10\%$  regardless of the current load demand.
- (2) Ensure frequency separation to power sources, *i.e.*, each power source supplies power with respect to its frequency characteristic. That is achieved due to the choice of weighting functions associated to  $H_\infty$  control design.
- (3) Regulate the supercapacitor state of charge to 50% which allows to absorb/provide power to fulfill instantaneous load power demand.
- (4) Impose a desired steady-state behavior for the rest of the power sources, *i.e.*, fuel cell and battery. This is equivalent to impose a certain power sharing demand between the two sources in steady-state

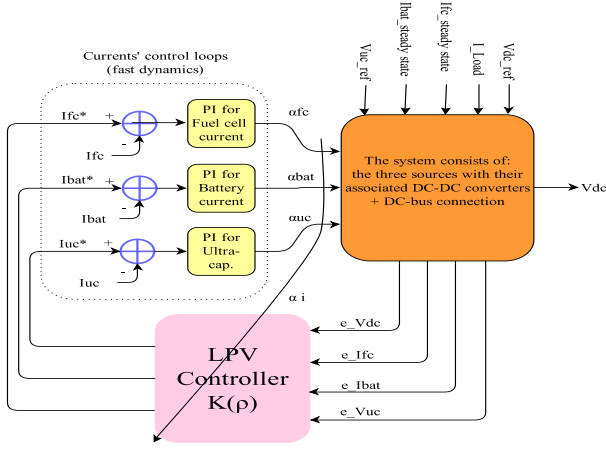


Figure 2. Global control block diagram.

### 2.3 LPV/ $H_\infty$ controller synthesis

In Nwesaty et al. [2014], an  $H_\infty$  control approach is developed to ensure the previous control objectives for system (1). The design of this controller is based on the general control configuration in Fig. 3, where several weighting functions are considered to handle the performance objectives such as DC-bus voltage tracking and frequency separation.

System in (1) can be rewritten under the generalized LPV MIMO system as follows:

$$P(\rho) : \begin{bmatrix} \dot{x} \\ z \\ y \end{bmatrix} = \begin{bmatrix} A & B_1 & B_2(\rho) \\ C_1 & D_{11} & D_{12} \\ C_2 & D_{21} & D_{22} \end{bmatrix} \begin{bmatrix} x \\ \omega \\ u \end{bmatrix} \quad (2)$$

In the considered approach each parameter  $\rho_i$  is assumed to be bounded by  $[0.1, 0.9]$  (this corresponds to the duty ratio accepted variation from 10% to 90%). Each parameter is supposed to be independent from the other parameters, and the system can be represented under a polytopic form with  $2^3 = 8$  vertices.  $B_2(\rho)$  depends on the parameter vector  $\rho$  which leads to use some filter in order to get a simple parameter-independent matrix as in Poussot-Vassal [2008].

The LTI weighting functions used for  $H_\infty$  optimization process are found using genetic algorithm (see Nwesaty et al. [2014]) and they are given as:

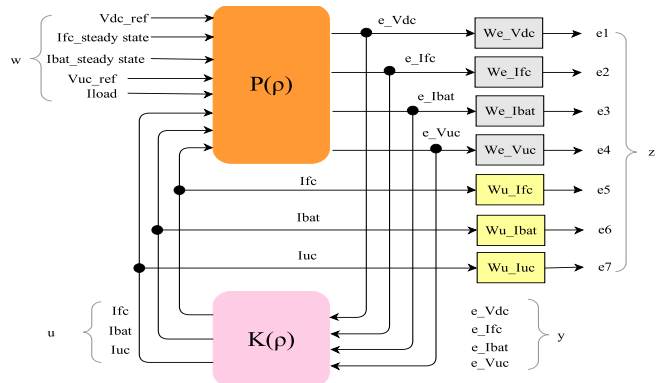


Figure 3.  $H_\infty$  Robust control design block diagram.

$$\left\{ \begin{array}{l} W_{eV_{dc}} = \frac{s/M_s + \omega_b}{s + \omega_b \cdot \epsilon} = \frac{0.5363s + 500}{s + 0.05} \\ W_{eI_{fc}} = 0.33 \\ W_{eI_{bat}} = 0.53 \\ W_{eV_{sc}} = \frac{s/M_s + \omega_b}{s + \omega_b \cdot \epsilon} = \frac{0.5263s + 0.05}{s + 0.0005} \\ W_{uI_{fc}} = \frac{s + \omega_{BC}/M_u}{\epsilon \cdot s + \omega_{BC}} = \frac{s + 0.0007}{0.9091s + 0.07} \\ W_{uI_{bat}} = \left( \frac{s + \omega_{BC}/M}{\epsilon \cdot s + \omega_{BC}} \times \frac{s/M + \omega_b}{s + \omega_b \cdot \epsilon} \right)^2 \\ = \left( \frac{s + 0.02}{0.035 \cdot s + 1} \times \frac{0.02 \cdot s + 0.001}{s + 3.5 \times 10^{-5}} \right)^2 \\ W_{uI_{sc}} = \left( \frac{s + \omega_{BC}/M}{\epsilon \cdot s + \omega_{BC}} \times \frac{s/M + \omega_b}{s + \omega_b \cdot \epsilon} \right)^2 \\ = \left( \frac{s + 0.428}{0.076 \cdot s + 15} \times \frac{0.028 \cdot s + 2}{s + 0.152} \right)^2 \end{array} \right. \quad (3)$$

In Nwesaty et al. [2014], the polytopic approach is used to find the desired LPV/ $H_\infty$  controller (Scherer et al. [1997]). According to the methodological framework of quadratic stabilization described in (Apkarian et al. [1995]), the problem is treated off line by solving a set of LMIs (convex optimisation using single Lyapunov function) at the vertices of the polytope. This gives the vertex controllers

$$K_i = \begin{bmatrix} A_i & B_i \\ C_i & D_i \end{bmatrix} \text{ with } 1 \leq i \leq 8. \text{ The LPV controller } K(\rho)$$

is computed on line as a convex combination of the vertex controllers  $K_i$  as follows:

$$K(\rho) = \sum_1^8 \alpha_i(\rho) K_i \quad (4)$$

with:

$$\alpha_i(\rho) = \frac{\prod_{j=1}^3 |\rho_j - \underline{C}(w_i)_j|}{\prod_{j=1}^3 |\bar{\rho}_j - \underline{\rho}_j|} > 0, \quad \sum_1^8 \alpha_i = 1$$

where  $\omega_i$  are the extremities of the polytope formed by the extreme values of the parameter vector  $\rho$ .  $C(w_i)_j$  is the  $j^{th}$  component of the vector  $C(w_i)$ ; it is defined as:

$$C(w_i)_j = \begin{cases} \bar{\rho}_j & \text{if } \omega_i = \rho_j \\ \underline{\rho}_j & \text{otherwise} \end{cases}$$

and in this application

$$\bar{\rho}_j = \max(\rho_j) = 0.9, \quad \underline{\rho}_j = \min(\rho_j) = 0.1$$

### 3. CONTROLLER ORDER-REDUCTION PROBLEM FORMULATION

The main idea of this paper concerns the order-reduction of the LPV/ $H_\infty$  controller. Indeed the LPV/ $H_\infty$  control synthesis gives eight MIMO vertex controllers each of which has eighteen dynamic states (144 states in total). An efficient controller order reduction will then facilitate its implementation in real on-board system with less need for powerful computation and memory resources. In this paper we will consider the order reduction of the vertex controller. Indeed the order reduction of a given LPV

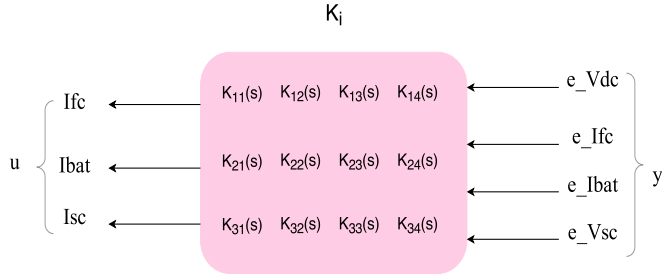


Figure 5. Transfer matrix of one vertex controller.

controller is a hard problem whose solution is not known today.

Although reducing the order of the vertex controllers is different from LPV control order-reduction, we will show that the reduced LPV controller (obtained as the combination of the reduced LTI vertex controllers) preserves stability and performances of the closed-loop system.

Fig. 5 shows the transfer matrix structure of a MIMO vertex controller, with 4 inputs and 3 outputs. One can notice that each entry  $K_{il,j}$  (where  $1 \leq i \leq 3$ ,  $1 \leq j \leq 4$ ) of the matrix is a SISO system.

Moreover, the  $K_i$  vertex controller can also be expressed by the following state-space representation:

$$K_i : \begin{cases} \dot{x}_c(t) = A_i x_c(t) + B_i y(t) \\ u(t) = C_i x_c(t) + D_i y(t) \end{cases}$$

where

$$A_i \in \mathbb{R}^{n \times n}, B_i \in \mathbb{R}^{n \times 4}, C_i \in \mathbb{R}^{3 \times n}, D_i \in \mathbb{R}^{3 \times 4}$$

with  $n = 18$

Let us denote the desired reduced-order controller as:

$$\hat{K}_i : \begin{cases} \dot{\hat{x}}_c(t) = \hat{A}_i \hat{x}_c(t) + \hat{B}_i y(t) \\ u(t) = \hat{C}_i \hat{x}_c(t) + \hat{D}_i y(t) \end{cases}$$

where

$$\hat{A}_i \in \mathbb{R}^{r \times r}, \hat{B}_i \in \mathbb{R}^{r \times 4}, \hat{C}_i \in \mathbb{R}^{3 \times r}, \hat{D}_i \in \mathbb{R}^{3 \times 4}$$

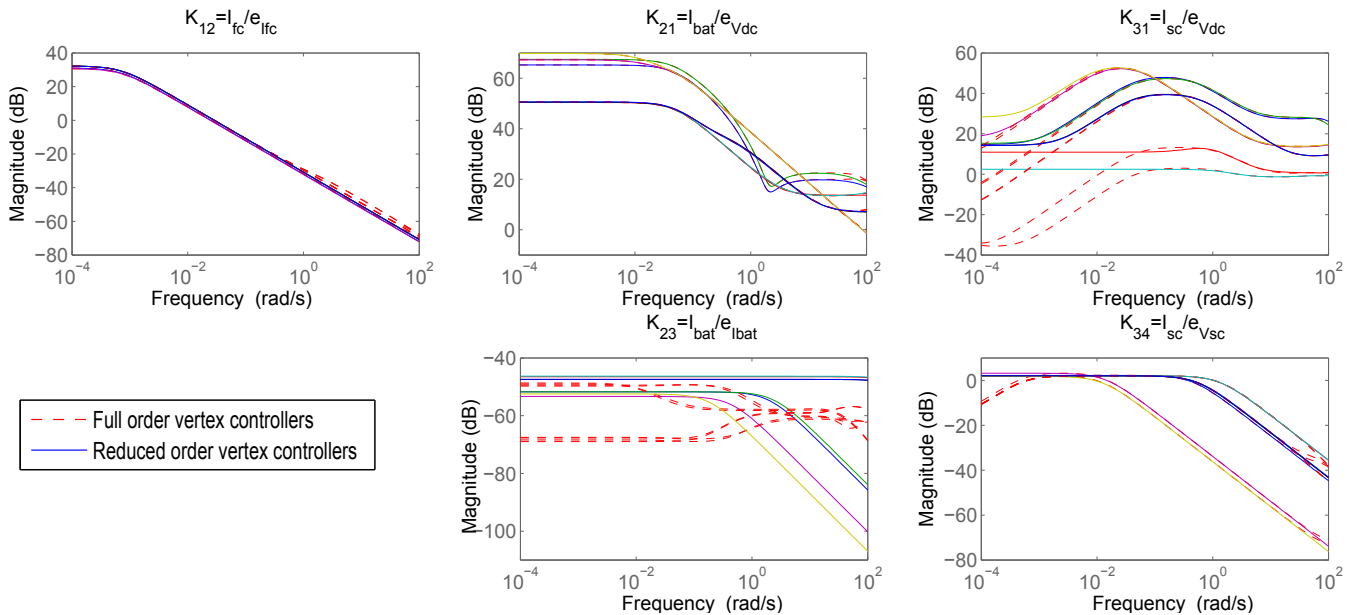


Figure 4. Frequency analysis comparison between full-order and reduced-order controllers.

and  $r < n$  is the reduced controller order.

The problem under consideration is then: find an integer  $r$  and matrices  $\hat{A}_i, \hat{B}_i, \hat{C}_i, \hat{D}_i$  such that  $\|K_i(s) - \hat{K}_i(s)\|$  is small with respect to a certain norm. MORE toolbox is used for this purpose under MATLAB<sup>®</sup> environment. For more details please refer to Poussot-Vassal and Vuillemin [2012]. For sake of simplicity, all vertex controllers are considered to have the same reduced order  $r$ . The Iterative SVD Tangential Krylov Algorithm (ISTIA) is used in this context because of its ability to handle MIMO problems and to preserve stability for reduced-order system as explained in (Poussot-Vassal and Vuillemin [2012]). Furthermore, according to the considered control problem where the frequency separation of the power sources is required, it is important to evaluate the controller order reduction effect over some predefined frequency range. Therefore  $\mathcal{H}_{2,\Omega}$  norm is the best choice in this case since it allows to preserve frequency characteristics found in Section 2 with respect to bandwidth frequency range  $\Omega$  of the closed-loop system. Below, ISTIA is applied for each vertex controller and is associated with  $\mathcal{H}_{2,\Omega}$  norm. Vertex controller are reduced for bandwidth of the system to order  $r = 11$  with negligible maximum error  $\sup_i \|K_i(s) - \hat{K}_i(s)\|_{\mathcal{H}_{2,\Omega}}$  with

$$\Omega = [0, 30] \text{ rad/sec}.$$

At this stage, the transfer matrix of the reduced-order controller becomes:

$$u = \begin{bmatrix} \sim 0 & K_{12} & \sim 0 & \sim 0 \\ K_{21} & \sim 0 & K_{23} & \sim 0 \\ K_{31} & \sim 0 & \sim 0 & K_{34} \end{bmatrix} y \quad (5)$$

where  $y = [e_{Vdc} \ e_{I_{fc}} \ e_{I_{bat}} \ e_{V_{sc}}]^T$  is the feedback error vector corresponds to DC-bus voltage, fuel cell steady-state current, battery steady-state current and supercapacitor SOC, respectively,  $u$  is the control input contains sources currents (Fig. 5). according to (5) one can notice that some entries of the transfer matrix  $K_{il,j}$  vanish. It is worth nothing that, this new form of the transfer matrix

can be explained regarding the physical properties of the studied system where:

- supercapacitor reacts with the DC-bus voltage error  $e_{V_{dc}}$  and its SOC steady-state error which is represented directly by supercapacitor voltage  $e_{V_{sc}}$ . That explains the existence of  $K_{31} = \frac{I_{sc}}{e_{V_{dc}}}$  and  $K_{34} = \frac{I_{sc}}{e_{V_{sc}}}$ , respectively.
- also for the previous reasons, battery reacts with the DC-bus voltage error  $e_{V_{dc}}$  and its steady-state current error. That explains the existence of  $K_{21} = \frac{I_{bat}}{e_{V_{dc}}}$  and  $K_{23} = \frac{I_{bat}}{e_{I_{bat}}}$ , respectively.
- the fuel cell reacts only with its steady-state current error but not with  $e_{V_{dc}}$  taking into consideration the fact that  $I_{fc} + I_{bat} + I_{sc} = I_{load}$ . That explains the existence of  $K_{12} = \frac{I_{fc}}{e_{I_{fc}}}$

Although there is no proof to guarantee the global LPV system stability by using ISTIA, the closed-loop quadratic stability is proved by the existence of the single Lyapunov function  $P > 0$  where  $A_i^T P + P A_i < 0$ ,  $1 \leq i \leq 8$

*Remark:* There exist also another powerful tool named Descent Algorithm for Residues and Poles Optimization (DARPO) that could be used instead of ISTIA. This method allows to determine the optimal reduced-order  $r$  by defining an accepted threshold limit for the error  $|K_i - \hat{K}_i|$ , which is found to be also  $r = 11$ .

#### 4. REDUCED-ORDER CONTROLLER FREQUENCY ANALYSIS

This section is dedicated to the comparison of the reduced-order  $LPV/H_\infty$  controller with the original one. The comparison is performed in frequency domain. Norm calculations will show the distance between the two closed-loop systems (using reduced-order controller and the full-order one).

Fig. 4 illustrates the frequency analysis of the  $K_i$  vertex controller and the reduced-order ones taking into consideration the Bode diagram for each SISO element  $K_{i,l,j}$ . One can notice that order-reduction respects the prespecified frequency intervals for each power source. For the tracking of the DC-bus voltage reference, supercapacitor ( $K_{31}$ ) is reduced for relatively high frequency, whereas the battery ( $K_{21}$ ) is reduced for low and mid-range frequency interval. On the other hand, steady-state behaviors for fuel cell ( $K_{12}$ ), battery ( $K_{23}$ ) and supercapacitor ( $K_{34}$ ) are reduced to low-pass first order systems.

Below the  $\mathcal{H}_\infty$  and  $\mathcal{H}_2$  norms of the controllers are calculated in order to illustrate the differences between the reduced-order and full-order controllers. Besides, the relative error between the two systems is also calculated using both  $\mathcal{H}_\infty$  and  $\mathcal{H}_2$ . Norms are illustrated in the following tables:

Table 1.  $\mathcal{H}_\infty, \mathcal{H}_2$  Norms calculations for both reduced and full-order controllers.

	$\mathcal{H}_\infty$	$\mathcal{H}_2$
Full-order controller O(18)	59.55	0.9041
Reduced-order controller O(11)	59.08	0.9378

Table 2. Relative errors between reduced and full-order controllers using  $\mathcal{H}_\infty, \mathcal{H}_2$  Norms.

Relative error	
$\frac{\left  \sup_i \ K_i\ _\infty - \sup_i \ \hat{K}_i\ _\infty \right }{\sup_i \ K_i\ _\infty}$	$7.942 \times 10^{-3}$
$\frac{\left  \sup_i \ K_i\ _2 - \sup_i \ \hat{K}_i\ _2 \right }{\sup_i \ K_i\ _2}$	$3.592 \times 10^{-2}$

#### 5. SIMULATION

In this section, a numerical simulation is performed to assess the performance of the global control structure in Fig. 2 by using the reduced order controller. Simulation is made using a nonlinear model for different parts of the electrical system including the power sources with their associated DC-DC converters. The Normalized European Driving Cycle (NEDC) is used as load power profile. Fig. 6 shows the load current, which is an image of the vehicle speed. The NEDC represents various driving conditions including acceleration, deceleration, fixed-speed and full-brake and allow assessing performance of DC-bus voltage regulation and evaluating the way how the three sources are coordinated to provide the demanded power.

The results are presented in Fig. 7. One can see that the system is able to provide the demanded power, while the DC-bus voltage shown in Fig. 7.a is well regulated at voltage reference 150 V within the allowed error of 10%. Fig. 7.c shows how power sources are coordinated in order to satisfy the system needs, with fuel cell supplying the average current and supercapacitor handling the peak variations, while the battery provides the midrange-frequency current. Currents' frequency analysis is also made in Fig. 7.d, where the power spectral density of each source current is computed, and normalized with respect to the maximum power delivered by each source. The remaining control objective is also satisfied in Fig. 7.b, where supercapacitor SOC is maintained within admissible range of  $[0,100]\%$ .

The reduced-order  $LPV/H_\infty$  controller satisfies the control objectives with a minor loss in the performance compared to the full-order one developed in Nwesaty et al. [2014].

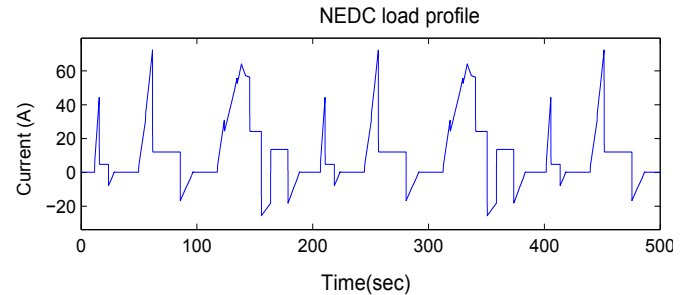


Figure 6. NEDC load current profile used in simulation.

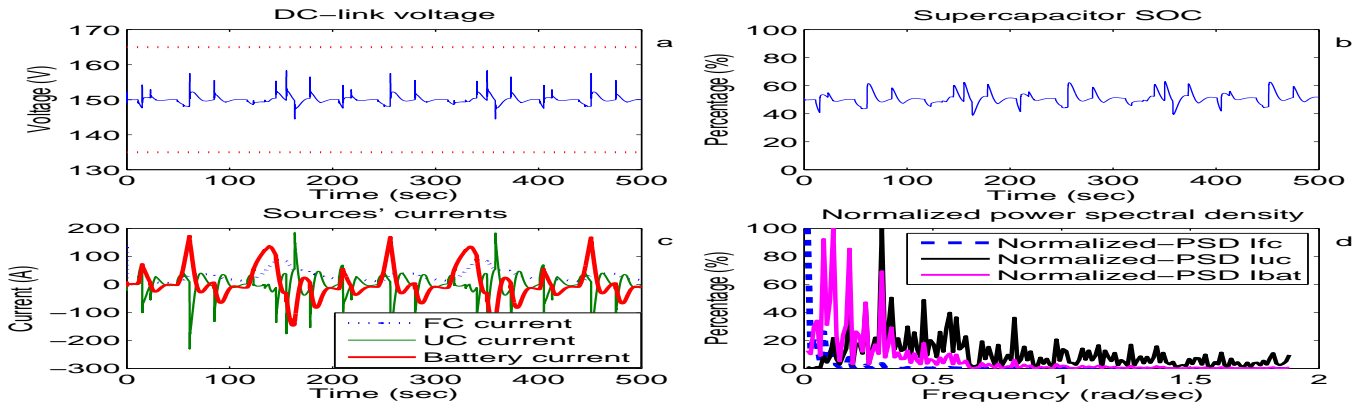


Figure 7. NEDC simulation results.

## 6. CONCLUSION AND FUTURE WORK

This paper presented the application of a reduction order method for a multi-variable LPV/ $H_\infty$  controller. The studied system is a multi-source energy system composed of three different kinds of power sources (fuel cell, battery and supercapacitor) on board of an electric vehicle. To meet the closed-loop system requirements the LPV controller was designed using a frequency-separation method achieved by using weighting functions associated to  $H_\infty$  optimization problem. The reduction approach was then dedicated to the simplification of the eight vertex controllers each of which being a LTI system of eighteen state variables, using some physical knowledge on the input/output properties. The reduced LPV controller ensures the quadratic closed-loop stability (as done by the full-order one) through the existence of a single Lyapunov function for all operating points, which greatly simplifies the implementation step while keeping the closed-loop performances.

The nonlinear electrical system has been simulated upon the Normalized European Driving Cycle (NEDC). Numerical simulation results show that where the control objectives are well satisfied for the reduced controller, in spite of a slight degradation compared to the original full-order LPV controller.

In future work more emphasis will be put on the physical properties of the studied system, in order to propose a fixed control structure corresponding to the number of power sources. A structured  $H_\infty$  design could be investigated in this application which could be useful from the generalization of the proposed power sharing control strategy point of view.

## REFERENCES

- I. Aharon and A. Kuperman. Topological overview of powertrains for battery-powered vehicles with range extenders. *IEEE Transactions on Power Electronics*, 26(3):868–876, March 2011.
- P. Apkarian, P. Gahinet, and G. Becker. Self-scheduled  $H_\infty$  control of linear parameter-varying systems: a design example. *Automatica*, 31(9):1251–1261, September 1995.
- K. J. Aström and T. Hägglund. *PID Controllers: Theory, Design, and Tuning*. Instrument Society of America, Research Triangle Park, NC, 2 edition, 1995.
- A. Fadel and B. Zhou. An experimental and analytical comparison study of power management methodologies of fuel cell, battery hybrid vehicles. *Journal of Power Sources*, 196(6):3271–3279, March 2011.
- A. Florescu, A.I. Bratcu, I. Munteanu, A. Rumeau, and S. Bacha. LQG optimal control applied to on-board energy management system of all-electric vehicles. *IEEE Transactions on Control Systems Technology*, PP(99):1–1, 2014. doi: 10.1109/TCST.2014.2372472.
- A. Florescu, S. Bacha, I. Munteanu, A.I. Bratcu, and A. Rumeau. Adaptive frequency-separation-based energy management system for electric vehicles. *Journal of Power Sources*, 280:410–421, April 2015.
- M.A. Hannan, F.A. Azidin, and A. Mohamed. Analysis of multi-power sources energy management system for electric hybrid vehicle. In *2011 IEEE Ninth International Conference on Power Electronics and Drive Systems (PEDS)*, pages 452–458, December 2011.
- A. Kuperman and I. Aharon. Battery/ultracapacitor hybrids for pulsed current loads: A review. *Renewable and Sustainable Energy Reviews*, 15(2):981–992, February 2011.
- W. Nwesaty, A.I. Bratcu, and O. Sename. Optimal frequency separation of power sources by multivariable LPV/ $H_\infty$  control: application to on-board energy management systems of electric vehicles. *53rd IEEE Conference on Decision and Control ({CDC})*, pages 5636–5641, 2014.
- C. Poussot-Vassal. *Multi-variable LPV robust control for vehicle chassis (Commande Robuste LPV Multivariable de Chassis Automobile)*. PhD thesis, Grenoble INP, Grenoble France, 2008.
- C. Poussot-Vassal and P. Vuillemin. Introduction to MORE: A Model REduction toolbox. In *2012 IEEE International Conference on Control Applications (CCA)*, pages 776–781, October 2012.
- C. Scherer, P. Gahinet, and M. Chilali. Multiobjective output-feedback control via LMI optimization. *IEEE Transactions on Automatic Control*, 42(7):896–911, July 1997.
- S.F. Tie and C.W. Tan. A review of energy sources and energy management system in electric vehicles. *Renewable and Sustainable Energy Reviews*, 20:82–102, April 2013.
- J. Wong, N.R.N. Idris, M. Anwar, and T. Taufik. A parallel energy-sharing control for fuel cell-battery-ultracapacitor hybrid vehicle. In *2011 IEEE Energy Conversion Congress and Exposition (ECCE)*, pages 2923–2929, September 2011.